NIPPON STEEL TECHNICAL REPORT No. 123 MARCH 2020

UDC 669 . 162 . 215 . 244

Technical Report

Development of Simulation Tool for Prediction of Burden Distribution by Using DEM and Its Comparing with Measurement Data of 1/3 Scale Experimental and Working Blast Furnaces

Hiroshi MIO* Masatomo KADOWAKI
Shinroku MATSUZAKI Toshiki NAKAUCHI
Yuuki KAWAGUCHI Takashi ENAKA

Abstract

The objective of this paper is the development of a prediction tool for burden distribution of a blast furnace by using the Discrete Element Method (DEM). The particle charging behavior via a rotating chute in a 1/3-scale experimental apparatus was recorded by a high-speed video camera, and the particle velocity was measured from the recorded images by using Particle Imaging Velocimetry (PIV). The particle trajectory discharged from the rotating chute was also measured in the experiment by inserting the rod, and the flow position was detected from the particle impact on the rod. The particle behavior was simulated by DEM, and it was validated by a comparison of the measurement results. The measurements of particle charging behavior were also conducted in Nagoya No. 3 Blast Furnace (BF), and the simulation results were compared with them. As a result, the simulated particle behavior correlated very well both in the 1/3-scale experiment and Nagoya No. 3 BF. Therefore, the simulation tool developed by this research is highly reliable when used for the prediction of particle trajectory in the blast furnace operation.

1. Introduction

Blast furnaces are countercurrent moving bed reactors for reducing iron ore to produce pig iron. As basic operations, ores, such as sinters, pellets, and lumps, are charged into the blast furnace with coke by stacking them alternatively, and the hot gas is blown from the tuyeres in the lower section of the blast furnace. The gas permeability in the blast furnaces is a significantly important factor and thereby maintaining the gas flow constant is essential for stable and high-efficiency operations. Therefore, controlling the process for charging raw materials (e.g., coke and sinter) into blast furnaces appropriately, or, controlling burden distribution, is very important. In recent years, bell-less type blast furnaces for which rotating chutes are used to charge raw materials into the blast furnaces have mainly been used. Nippon Steel Corporation uses many of these blast furnace types. In the charging process using the rotating chute, raw materials are charged targeting designated locations in the radial direction by rotating the chute a preset number of times while changing its tilting angle. The ore to coke mass ratio (O/C ratio) in the radial direction is controlled by changing the chute tilting angle and the number of rotations. Therefore, predicting onto which locations raw materials discharged from the rotating chute will land accurately improves burden distribution control. Researchers have been studying and developing many prediction models for burden distribution.[1–7] Many of such models simulate the motion of raw materials mathematically and they have been actively used in blast furnace operations. However, new burden distribution prediction models considering the influence of the physical properties of each raw material to be charged may be required because the burden distribution has been diversifying due to recent changes in raw materials. In addition, the specifications of equipment used to control burden distribution to a high degree should be studied using simulation. Therefore, there is a strong demand for kinetic simulation models that can

* Senior Researcher, Dr.(Eng.), Ironmaking Research Lab., Process Research Laboratories
20-1 Shintomi, Futtsu City, Chiba Pref. 293-8511

Fig. 1 Picture of 1/3 scale experimental apparatus for burden distribution

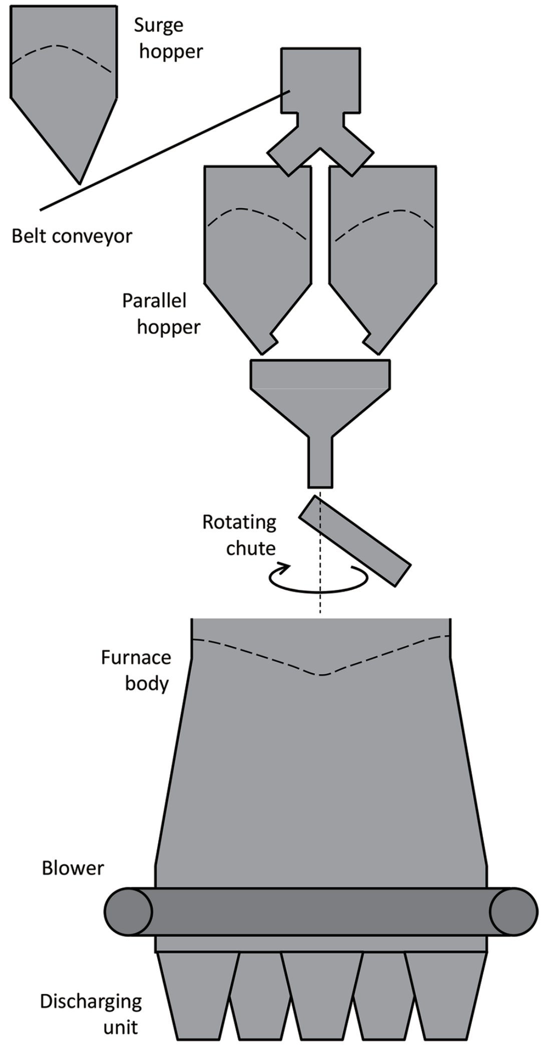

Fig. 2 Schematic illustration of 1/3 scale experimental apparatus

consider the physical properties of particles and detailed equipment requirements.

Nippon Steel has been developing burden distribution prediction models for blast furnaces using the Discrete Element Method (DEM)[8]—a particle behavior analysis technique. DEM handles particle behavior as a discrete system, calculates the force working on each particle, and analyzes the behavior of the entire particle group. This method has been applied to many particulate processes (e.g., mixing, grinding, particle transportation, charging, fluidized bed, and electrophotography).[9–17] Many studies have also been conducted for blast furnace processes.[18–28] Generally, particle behavior is very complicated and sometimes shows specific motion. Therefore, regarding simulation by DEM, only after the results have been verified by closely comparing them to actual phenomena can they be put to practical utilization.

In 2009, Nippon Steel set up a 1/3-scale bell-less type experimental blast furnace shown in **Fig. 1** to enhance the burden distribution research of the blast furnace and development. This 30-m high experimental apparatus is a furnace top model approximately 1/3 scale of Nagoya No. 3 Blast Furnace. As shown in **Fig. 2**, the model consists of a surge hopper, parallel hopper, rotating chute, and furnace body (only the top) and reproduces the raw material transportation and charging processes of working blast furnaces. The model has a blower in the lower section of the furnace body and a discharging unit at the bottom for considering the gas flow in the furnace and the burden descending behavior. Nippon Steel has been working to improve the accuracy of blast furnace burden distribution prediction models by DEM using this experimental apparatus.

This report compares the simulated charging behavior from the rotating chute of a bell-less type blast furnace and the behavior in the 1/3-scale experimental blast furnace,[28] along with the phenomena observed in Nagoya No. 3 Blast Furnace and measurement and verification results.[27]

2. Discrete Element Method

DEM determines all the kinematic force on each finite-sized particle and solves the equations of translational and rotational motion for each particle one by one for each micro time as its basic algorithm

$$\dot{\mathbf{v}} = \frac{\sum \mathbf{F}}{m}, \quad (1)$$

$$\dot{\boldsymbol{\omega}} = \frac{\sum \mathbf{M}}{I}. \quad (2)$$

Where, $\mathbf{v}$ is the particle velocity and $\boldsymbol{\omega}$ is its angular velocity. $\mathbf{F}$ and $\mathbf{M}$ are the force and the moment acting on the particle, respectively. m and I are the mass of the particle and the moment of inertia. In particle behavior analysis of the blast furnace charging process, the force, $\mathbf{F}$, is mainly the repulsive force when particles come into contact and gravity. For other particulate processes, various phenomena have been analyzed considering fluid drag force, magnetic force, electrostatic force, adhesion, and others. Regarding collision between particles or that between a particle and structure, plastic deformation and damage of the particle(s) are not considered and local overlap is tolerated. Thus, when the equation below holds, it is regarded that two particles have collided

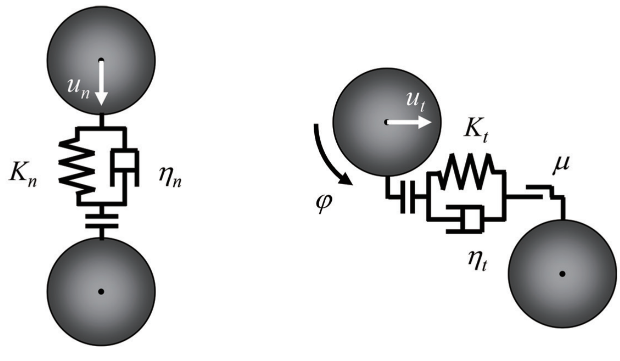

(a) Compressive force (b) Shear force

Fig. 3 Model for contact force

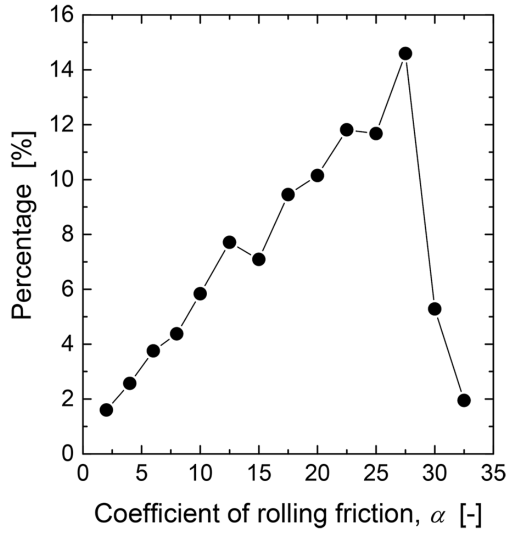

Fig. 4 Distribution of coefficient of rolling friction[29)]

$$d < r_i + r_j. \tag{3}$$

Where, d is the distance between the central coordinates of the two target particles, r is the particle radius, and i and j are particle numbers. The contact between the two particles is given by Voigt model, which consists of a spring-dashpot as shown in **Fig. 3**, not by a perfectly elastic collision. The elastic and inelastic properties of the particles are expressed by the elastic spring (elastic coefficient: K) and viscous dashpots (viscous coefficient: η) inserted between the contact points. In addition, to express the frictional interaction due to the contact of the particles, a slider for the friction (frictional coefficient: μ) has been inserted in the shear direction. The force acting on the contact surface of the particles in the nominal direction $\mathbf{F}_{\mathrm{n}}$ and that in the sharing direction $\mathbf{F}_{\mathrm{t}}$ can be calculated using the following equations

$$\mathbf{F}_{n,ij} = \left(K_n \Delta u_{n,ij} + \eta_n \frac{\Delta u_{n,ij}}{\Delta t} \right) \mathbf{n}_{ij}, \tag{4}$$

$$\mathbf{F}_{t,ij} = \min \left\{ \mu \left| \mathrm{F}_{n,ij} \right| \mathbf{t}_{ij}, \left[K_t \left(\Delta u_{t,ij} + \Delta\varphi_{ij} \right) + \eta_t \left(\frac{\Delta u_{t,ij} + \Delta\varphi_{ij}}{\Delta t} \right) \right] \mathbf{t}_{ij} \right\}. \tag{5}$$

Where, u and φ are relative displacement at the contact point of the two particles caused by the translation and rotation, respectively. **n** and **t** denote the unit vector of the normal and tangential components. The contact force and moment between particle i and all the other particles that come into contact with particle i are calculated, they are added, the translational and the angular velocities are calculated, and the displacement of particle i from t to $t+\Delta t$ is calculated. These processes are looped for all particles until $t=t_{\mathrm{max}}$ to simulate the behavior of the entire particle group.

Generally, DEM regards a particle as a sphere. However, most particles (analysis targets) are nonspherical. Therefore, the resistance is often given to the rotational motion of particles to consider their shape. In this study, the rolling friction (moment) expressed as the following equation was applied to the particles

$$\mathbf{M}_{r,i} = -\frac{3}{8} \alpha_i b \left| \mathbf{F}_n \right| \frac{\boldsymbol{\omega}_i}{\left| \boldsymbol{\omega}_i \right|}. \tag{6}$$

Where, b is a radius of the contact surface, and α denotes the coefficient of rolling friction. The shape of the sinter and coke particles in this study cannot all be identical. Therefore, every particle in this study has a different coefficient of rolling friction in DEM such that each shows different rolling behavior. The distribution of α (**Fig. 4**) was determined based on a previous study:[29)] A single particle was dropped onto an inclined plane to obtain the distribution of the rolling distance and its trend was compared to the behavior of the particle when it entered the chute.

3. Experimental Conditions

3.1 1/3-scale experiment

The 1/3-scale burden distribution experimental blast furnace was used to measure the particle behavior and a trajectory through the rotating chute and the results were compared with the simulation results by DEM to verify the consistency. Sinter particles in 5 to 10 mm (57.3 mass%) were mixed with those in 10 to 20 mm (42.7 mass%). The raw materials were charged from the surge hopper to the parallel hopper and then discharged from the parallel hopper at a mass flow rate of 60.2 kg/s into the blast furnace via the rotating chute. The behavior of particles discharged from the rotating chute was recorded with a high-speed video camera (HiSpec, Fastec Imaging). Particles coming towards the camera were recorded from one side of the rotating chute at a recording rate of 1 000 fps. The particle velocity was measured from the images using the particle image velocimetry (PIV) and software (Flow-PIV ver. 2.2, Library Co., Ltd.).

The particle trajectory after discharge from the rotating chute was also measured using a metering rod. The rod was inserted into the blast furnace as shown in **Fig. 5** to detect particle passing positions in two levels based on the impact of particles on it. The rod angles were 0 and 30 degrees. A pressure sensitive sheet (PRESCALE, FUJIFILM Corporation) was put on the rod surface to quantify the impact stress. The color of the sheet changed when the discharged particles impacted on it. The pressure values were analyzed using a special scanner and software (FPD-9270, FUJIFILM Corporation). The chute rotational speed was 13.4 rpm and the chute tilting angles were 51.1 to 41.2 degrees.

3.2 Working blast furnace test

High-speed video recording was carried out during a shutdown at Nagoya No. 3 Blast Furnace and the discharging behavior from the rotating chute and particle trajectory were recorded. A manhole was opened during shutdown as shown in **Fig. 6**. The camera was the same as that used in the 1/3-scale experiment and particles traveling toward the camera were recorded from the side view angle as well. The frame rate of high-speed recording was set to 1 500 fps. Sinter particles were charged at the mass flow rate of 0.67 t/s. The

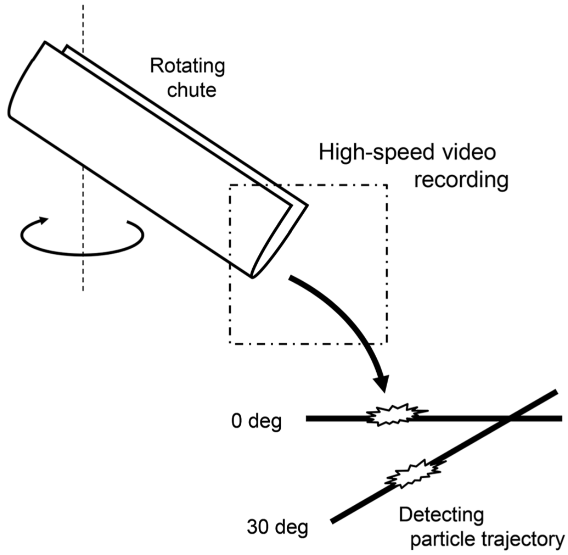

Fig. 5 Schematic illustration of the setup for 1/3 scale experiment

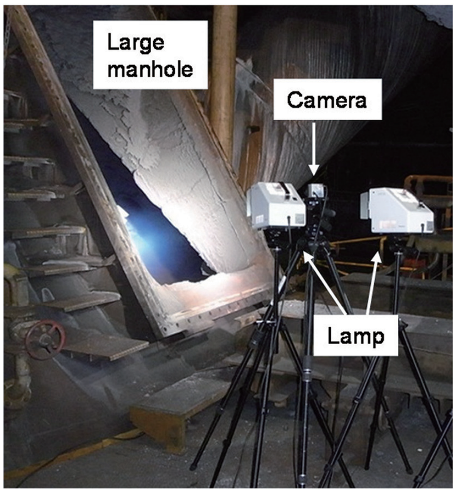

Fig. 6 Picture of setup of high-speed video camera in Nagoya No. 3 BF[27)]

chute tilting angle was 51.1 degrees and the rotational speed of the chute was 8 rpm. After the recording, the particle velocity was analyzed by PIV. Particle trajectory was also measured using a metering rod as shown in **Fig. 7** as is the case with the 1/3-scale experiment. The falling particles impacted on the rod were inserted into the blast furnace at an angle of 35 degrees. A pressure sensitive sheet was placed on the rod surface. The chute tilting angles were 51.1 and 38.8 degrees.

4. Simulation Conditions

The behavior of sinter particles charged into a furnace through a rotating chute was simulated by DEM and the simulation results were compared with the experimental results at the 1/3-scale experimental blast furnace and Nagoya No. 3 Blast Furnace. The charging conditions in the simulation, such as equipment specifications (e.g., length of the rotating chute), mass flow rate, and rotational speed, are equal to those in the 1/3-scale experiment and working blast furnace test. The density of sinter was 3300 kg/m^3, Young's modulus was 3.5 GPa, and Poisson's ratio was 0.25. The particle diameter in the 1/3-scale experiment was 5 to 20 mm and 10 to 35 mm in the working blast furnace test. **Tables 1** and **2** list detailed particle diameter distribution and number of particles. Every particle has a different coefficient of rolling friction as described regarding Equation (6) to consider differences of the shapes between particles. The coefficient of rolling friction for each particle was set by generating a random number at the beginning of the simulation with their distribution corresponding to Fig. 4. The simulation was processed by shared memory parallel computation with OpenMP to analyze particle behavior for one rotation.

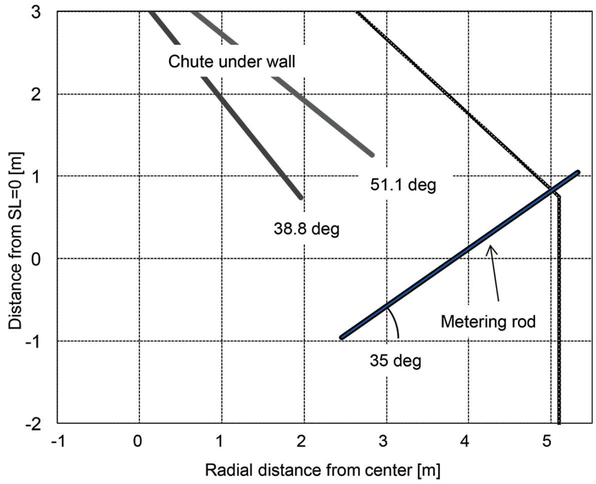

Fig. 7 Schematic illustration of position relation for the rod and chute under wall in Nagoya No. 3 BF[27)]

Table 1 Particle conditions in DEM for 1/3 scale experimental apparatus

Particle size [mm]	Number of particles [-]	Mass fraction [-]
5	196079	0.142
7.5	58097	0.142
9.5	28587	0.142
10.5	17087	0.115
12.5	10127	0.115
15	5860	0.115
17.5	3690	0.115
20	2472	0.115

Table 2 Particle conditions in DEM for Nagoya No. 3 BF[27)]

Particle size [mm]	Number of particles [-]	Mass fraction [-]
10	1017574	0.352
15	254393	0.297
25	50878	0.275
35	5191	0.077

5. Results and Discussions

5.1 Comparison with the 1/3-scale experiment

Figure 8 shows the behavior of the particles discharged from the rotating chute recorded by the high-speed video camera when the chute tilting angle was 51.1 degrees. The figure shows that the particles are pressed up against the chute side-wall due to the centrifugal force of the chute rotation. **Figure 9** shows the particle discharging behavior simulated by DEM. The snapshot shows that the particles are pressed up against the chute side-wall similar to that in the image taken by the high-speed video camera. Both results correlate well. The flow width at the outlet is 191 mm in the experiment and 187 mm in the simulation by DEM, so the values are almost the same. The value in the simulation by DEM is slightly smaller. This may be because the particles are regarded as spheres in the simulation, so the void between the particles is slightly smaller than the actual ones and thereby the height decreases.

Figure 10 shows an example of the analyzed results of the image taken by the high-speed video camera that were analyzed by PIV. The mean velocity of multiple images at the A-A line in the figure was regarded as the discharging velocity at the tilting angle. The particles when the rotating chute positioned itself just beside the camera were analyzed. In addition, PIV analysis can basically measure only the velocity of the flow surface. Therefore, the discharging velocity of the particles on the flow surface (camera side) was analyzed in the simulation. **Table 3** lists the mean discharging velocity. The table shows that the discharging velocity increases as the tilting angle gets smaller. This is because as the chute angle approaches the vertical angle, the deceleration during the drop into the chute becomes smaller and the influence of gravity when particles move in the chute increases. The table shows that the simulation results by DEM mostly agree with the experimental values, confirming that the simulation reproduces the behavior well.

Figure 11 shows an image of the particle trajectory measurement system. The image shows that the particles discharged from the rotating chute are striking the metering rod inserted from the right side (angle: 0 degrees). After the impact, the rod was extracted and the pressure sensitive sheet was peeled and scanned with a special scanner. **Figure 12** shows an example of impact stress distribution. The impact force distribution along the length of the rod was

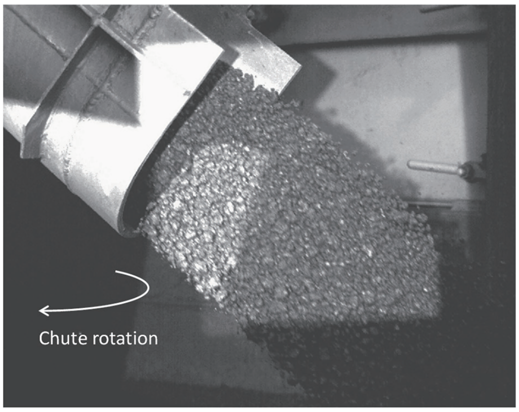

Fig. 8 Recorded image of particle discharging behavior from the rotating chute in 1/3 scale experiment

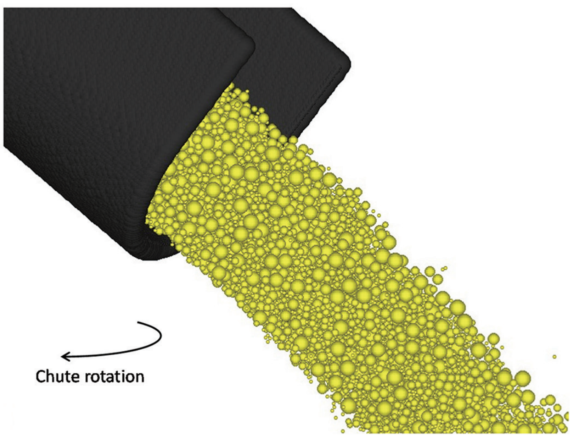

Fig. 9 Snapshot of particle discharging behavior simulated by DEM

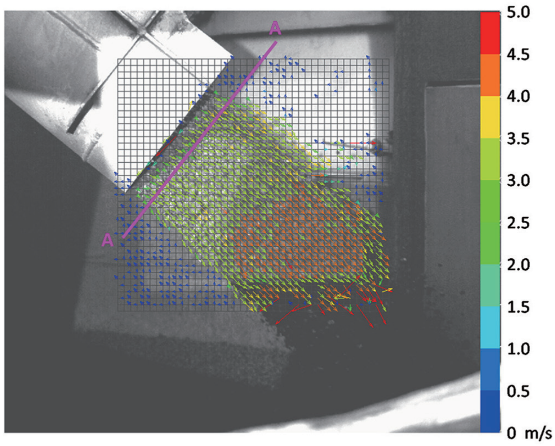

Fig. 10 Particle discharging velocity field by PIV

Table 3 Comparison of particle discharging velocity

Chute inclination angle [deg]		51.1	49.3	47.4
Particle velocity [m/s]	Measured (1/3 scale)	3.11	3.13	3.21
	Simulated (DEM)	3.02	3.15	3.26

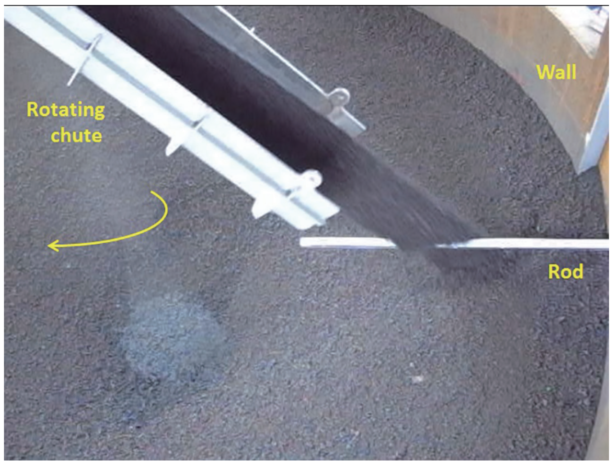

Fig. 11 Picture of measuring the particle trajectory in 1/3 scale experiment

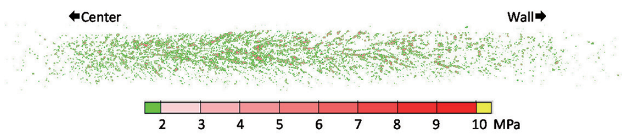

Fig. 12 Typical example of the impact stress distribution

calculated based on the obtained pressure values and evaluated as the downflow distribution in the radius direction. **Figure 13** shows the impact stress distribution with the chute tilting angle of 47.4 degrees and the rod insert angle of 0 degrees. The figure shows that the downflow passes the area ranging from approximately 300 to 600 mm from the wall. The simulation results that are also shown in Fig. 13 show the mass distribution of the particles that pass the position of the metering rod in the longitudinal direction of the rod. The figures confirm that both results are almost identical.

Figure 14 shows snapshots of particle trajectory simulated with the chute tilting angle of 47.4 and 41.2 along with the impact positions of the downflow obtained in the 1/3-scale experiment. The impact range in the experiment was where the cumulative impact force was 2.275 to 97.725%. The flow positions for 50% were determined to be the mainflow and plotted in the figure. The figures show that the impact positions in the experiment (at 0 and 30 degrees on the metering rod) correlate very well with the simulated trajectory.

At the tilting angle of 41.2 degrees, it seems that the upper layer of the flow is slightly different. This is because the particles in the upper layer of the flow have dispersed. They were detected as impact signs in the experiment; however, the simulation snapshot was taken only for a moment, which made it difficult to identify them. Meanwhile, the simulation image shows that the particles in the upper layer have also dispersed, so the results agree with each other. Therefore, the simulation by DEM can reproduce the discharging velocity from the rotating chute and particle trajectory in the 1/3-scale experiment well.

5.2 Comparison with Nagoya No. 3 Blast Furnace

Figure 15 shows the behavior of sinter particles discharged from the rotating chute recorded by a high-speed video camera at Nagoya No. 3 Blast Furnace. The behavior at the first rotation in which the influence of dust was small was recorded. The image clearly shows even individual particles. The discharged particles were pressed up to one side due to rotation of the chute as is the case with the 1/3-scale experiment. The scaled model results agree well with the working blast furnace test results. The simulated particle behavior shown in **Fig. 16** is similar to that in the recorded image in Fig. 15.

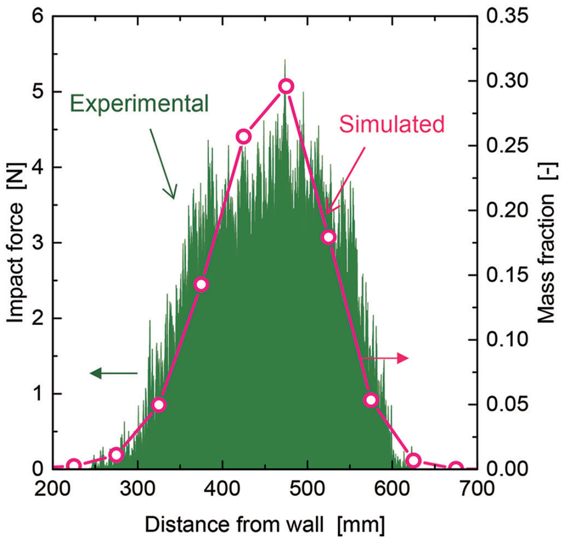

Fig. 13 Comparison of the impact stress distribution and the particle mass distribution under 47.4 deg in the chute angle and 0 deg in the rod insert angle

Figure 17 shows the analysis results of the high-speed video camera image analyzed by PIV and simulated particle velocity distribution at the time of discharge. Although some sections could not be analyzed due to halation in the PIV image, the two figures show the same tendency. The mean particle velocity after discharge from the chute is 4.75 m/s in the case of PIV and 4.69 m/s in the case of DEM. The two values are very close. Therefore, the simulation can reproduce the behavior under the blast furnace conditions well.

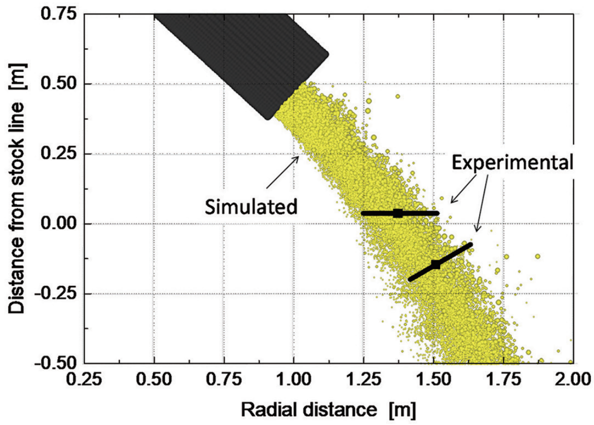

(a) 47.4 deg

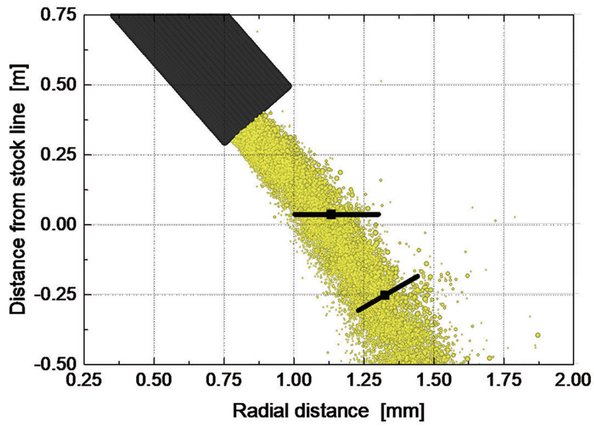

(b) 41.2 deg

Fig. 14 Comparison of particle trajectory

Fig. 15 Recorded images of charging sinter particles by high-speed video camera in Nagoya No. 3 BF[27)]

Figure 18 shows the results of the trajectory measurement using a metering rod inserted into the blast furnace. A pressure sensitive sheet was attached to the surface of the metering rod to measure impact positions as is the case with the 1/3-scale experiment. The figure shows the impact stress distribution to the distance from the tip of the metering rod. The figure also shows the simulated mass distribution of the particles passing the metering rod position. Although the distribution width in the blast furnace test is slightly wider, the two distribution forms correlate very well. The reason why the width in the blast furnace test results is wider may be because the particles flow in a rather dispersed state due to many factors that disturb the flow (e.g., wear of the liner inside the chute). **Figure 19** shows that the simulated discharging trajectory agrees well with the actual impact positions.

Thus, the particle trajectory simulation by DEM developed in

Fig. 16 Snapshot of particle charging behavior simulated by DEM[27)]

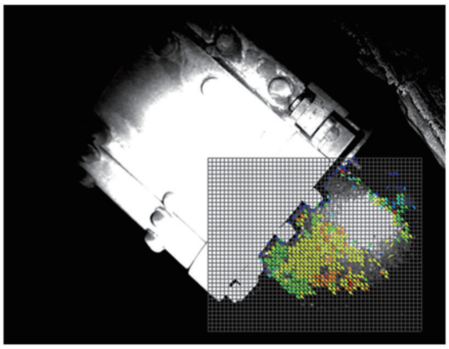

(a) PIV

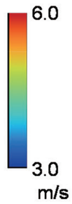

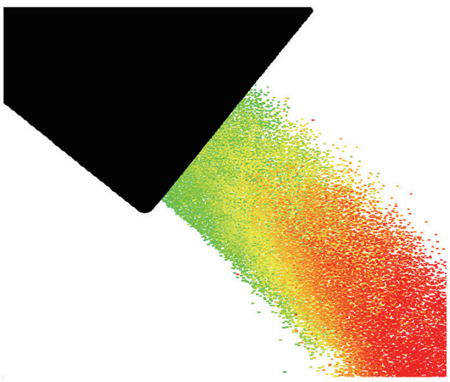

(b) DEM

Fig. 17 Particle velocity field around the rotating chute in Nagoya No. 3 BF[27)]

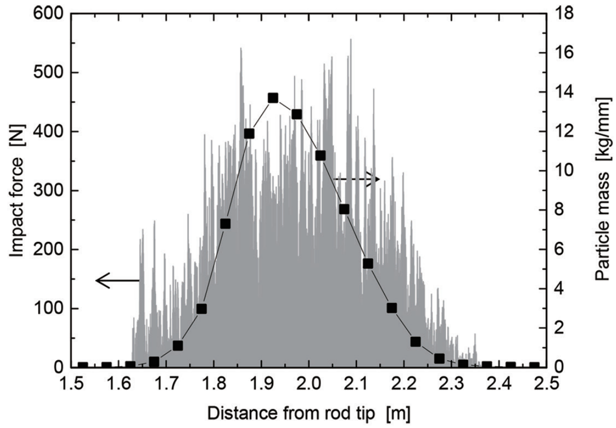

(a) 51.1 deg

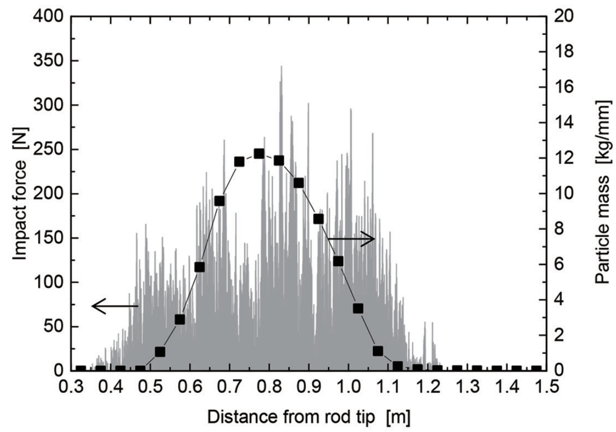

(b) 38.8 deg

Fig. 18 Comparison of the impact stress distribution and the particle mass distribution in Nagoya No. 3 BF[27)]

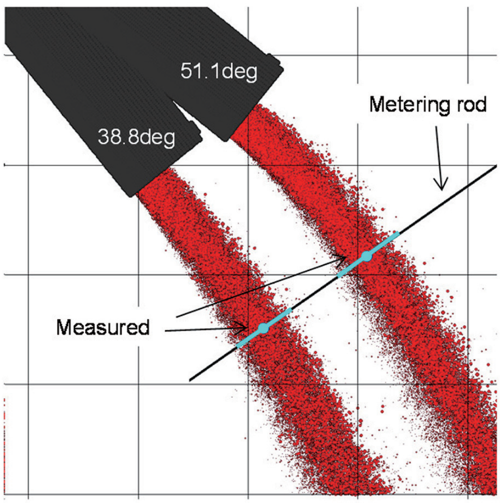

Fig. 19 Comparison of particle trajectory for Nagoya No. 3 BF[27)]

this study is highly accurate and thereby it can be sufficiently applied to the bell-less type blast furnace operation to predict and set the charging conditions.

6. Conclusion

This report introduced the charging behavior of particles discharged from the rotating chute of a bell-less type blast furnace simulated by DEM for the development of a burden distribution prediction model. To examine the simulation accuracy, a 1/3-scale experimental blast furnace was used to record particle discharging behavior from the rotating chute with a high-speed video camera to measure particle velocity. In addition, to compare the trajectory from the rotating chute, a metering rod was inserted into the furnace to measure the impact positions on the rod. Comparing the measured results to the simulation results by DEM indicates that the velocity and trajectory between the two cases have good correlation. In addition, the discharging behavior and trajectory were measured at Nagoya No. 3 Blast Furnace as well and the results were compared to the simulation results, showing an excellent correlation. These results confirm that the particle trajectory simulation by DEM developed in this study is highly accurate and thereby it can be sufficiently applied to bell-less type blast furnace operation design.

References

1) Kajiwara, Y. et al.: Trans. ISIJ. 24, 799 (1984)
2) Okuno, Y. et al.: Tetsu-to-Hagané. 73, 91 (1987)
3) Hattori, M. et al.: Tetsu-to-Hagané. 78, 1345 (1992)
4) Radhakrishnan, V. R., Ram, K. M.: J. Process Contr. 11, 565 (2001)
5) Nag, S. et al.: Ironmak. Steelmak. 36, 509 (2009)
6) Mitra, T., Saxén, H.: Metall. Mater. Trans. B. 45, 2382 (2014)
7) Fu, D. et al.: Appl. Math. Model. 39, 7554 (2015)
8) Cundall, P. A., Strack, O. D. L.: Geotechnique. 29, 47 (1979)
9) Bertrand, F. et al.: Chem. Eng. Sci. 60, 2517 (2005)
10) Moreno, R. et al.: Powder Technol. 130, 132 (2003)
11) Rajamani, R. K. et al.: Powder Technol. 109, 105 (2000)
12) Cleary, P. W., Sawley, M. L.: Appl. Math. Model. 26, 89 (2002)
13) Ketterhangen, W. R. et al.: Powder Technol. 179, 126 (2008)
14) Taberlet, N. et al.: Phys. Rev. E. 73, 050301 (2006)
15) Kaneko, Y. et al.: Chem. Eng. Sci. 54, 5809 (1999)
16) Kawaguchi, T. et al.: Powder Technol. 109, 3 (2000)
17) Severens, I. E. M. et al.: Granul. Matter. 8, 137 (2006)
18) Yuu, S. et al.: ISIJ Int. 45, 1406 (2005)
19) Zhou, Z. et al.: ISIJ Int. 45, 1828 (2005)
20) Nouchi, T. et al.: Tetsu-to-Hagané. 92, 955 (2006)
21) Mio, H. et al.: ISIJ Int. 47, 1745 (2007)
22) Mio, H. et al.: ISIJ Int. 49, 479 (2009)
23) Natsui, S. et al.: ISIJ Int. 51, 41 (2011)
24) Yu, Y., Saxén, H.: ISIJ Int. 52, 788 (2012)
25) Mio, H. et al.: Miner. Eng. 33, 27 (2012)
26) Kim, S. Y., Sasaki, Y.: ISIJ Int. 53, 2028 (2013)
27) Mio, H. et al.: ISIJ Int. 57, 272 (2017)
28) Mio, H. et al.: Powder Technol. 344, 797 (2019)
29) Mio, H. et al.: ISIJ Int. 48, 1696 (2008)

Hiroshi MIO
Senior Researcher, Dr.(Eng.)
Ironmaking Research Lab.
Process Research Laboratories
20-1 Shintomi, Futtsu City, Chiba Pref. 293-8511

Masatomo KADOWAKI
Senior Manager
Ironmaking Technology Div.

Shinroku MATSUZAKI
Senior Researcher, Dr.(Eng)
Ironmaking Research Lab.
Process Research Laboratories

Toshiki NAKAUCHI
Manager
Ironmaking Technology Dept.
Ironmaking Div.
Muroran Works

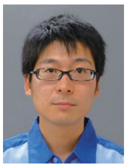

Yuuki KAWAGUCHI
Senior Manager
Ironmaking Technology Dept.
Ironmaking Div.
Nagoya Works

Takashi ENAKA
Senior Manager, Head of Mill
Blast Furnace Mill
Ironmaking Div.
Nagoya Works